

Flow of a model shear-thickening micellar fluid past a falling sphere

Shijian Wu and Hadi Mohammadigoushki*

*Department of Chemical and Biomedical Engineering, FAMU-FSU College of Engineering,
Florida State University, Tallahassee 32310, United States*



(Received 25 March 2019; published 19 July 2019)

We present quantitative measurements of a dilute micellar solution past a falling sphere. The dilute micellar solution that consists cetyltrimethylammonium bromide and 5-methyl salicylate (CTAB/5mS) in deionized water exhibits shear-thickening behavior beyond a critical shear rate of $\dot{\gamma}_c \approx 0.4$ (1/s). Previous experiments have demonstrated that this micellar solution forms unentangled rodlike micelles at equilibrium [Davies *et al.*, *J. Am. Chem. Soc.* **128**, 6669 (2006)]. At a vanishingly small Reynolds number $Re = 0.03$, the drag coefficient for the falling sphere is similar to that of a Newtonian fluid. However, surprisingly, for conditions that correspond to $0.09 \leq Re \leq 9.86$, falling spheres experience a significant drag reduction. Moreover, an unusually extended wake which spans over a long distance $>80a$ downstream of the sphere is detected by particle image velocimetry. These unusual results could be rationalized by invoking the phenomenon of flow-induced structure formation. We hypothesize that strong shear and/or extensional flows around the falling sphere could trigger aggregation of rodlike micelles into giant wormlike structures. Such wormlike micelles may induce significant sphere drag reduction and extended elastic wakes in the rear of sphere. This interpretation is consistent with the steady shear and transient extensional experiments, whereby a strong shear and elongational thickening have been recovered.

DOI: [10.1103/PhysRevFluids.4.073303](https://doi.org/10.1103/PhysRevFluids.4.073303)

I. INTRODUCTION

Flow past a falling sphere is one of the benchmark problems in both theoretical and experimental fluid mechanics [1,2]. The hydrodynamic mechanism of the Newtonian fluid past a falling sphere has received continuous attention since the pioneering work of Stokes and is relatively well understood [3]. However, most of industrial processes, such as oil recovery, waste water treatment, and food processing, involve interaction between falling spheres and non-Newtonian complex fluids. Inspired by these applications, multiple research groups have investigated effects of non-Newtonian features, including shear thinning [4–14], elasticity [15,16], and shear thickening [17–19] in flow of complex fluids past a falling sphere.

McKinley and colleagues studied flow of a single falling sphere past viscoelastic fluids [5,9]. While a negative wake forms in the rear of the falling sphere in shear-thinning polyacrylamide solution, an extended wake was observed for a constant viscosity polyisobutylene solution [5]. The negative wake is characterized by motion of the fluid in an opposite direction to that of the falling sphere. These researchers have shown that the strongest negative wake region occurs at locations downstream of the sphere where extensional flow is strongest. In addition, Fabris *et al.* [10] quantified the velocity field around a falling sphere in a constant viscosity elastic fluid based on monodisperse, high molecular weight polystyrene and showed formation of an extended wake

*Corresponding author: hadi.moham@fsu.edu

behind the falling sphere with no signs of negative velocities [10]. Verneuil *et al.* [20] studied a single-sphere sedimentation in a shear-thinning viscoelastic fluid based on xanthan gum and reported formation of a negative wake in the rear of the sphere. Therefore, it is believed that shear thinning contributes significantly to the formation of the negative wake structure.

Numerical simulations have also shown that negative wake can form behind a falling sphere in viscoelastic shear-thinning fluids when the ratio of Deborah number (De) to Trouton ratio (Tr) is beyond a critical threshold [6,8]. The Deborah number is defined as $De = \lambda \dot{\gamma}$ and the Trouton ratio is $Tr = \eta_E / \eta_0$. λ , $\dot{\gamma}$, η_E , and η_0 are the relaxation time, characteristic shear rate, transient extensional viscosity, and zero-shear rate viscosity of the fluid. $\dot{\gamma} = v_s/a$, where v_s and a are the terminal velocity and the diameter of the falling sphere, respectively.

Although effects of shear thinning and/or elasticity on the falling sphere problem have been extensively studied in the past, another important feature of complex fluids, shear thickening, has received much less attention. Shear-thickening behavior has been reported in a range of industrially important fluids such as concentrated suspensions. Perhaps one of the difficulties associated with sphere sedimentation studies of shear-thickening fluids is related to the opaque nature of these systems. Von Kann and colleagues studied sphere sedimentation in a shear-thickening corn-starch suspension. The authors used a thin rigid metal wire attached to the top of the falling sphere to track the sphere center of mass in the corn-starch suspension [19]. They showed that a falling sphere in this system never attains a constant terminal velocity; instead it experiences an oscillatory settling. The oscillatory behavior was partially explained by a jamming model [19]. We note that attaching a thin wire to the falling sphere may affect sphere sedimentation dynamics. Flow of shear-thickening fluids past a falling sphere has also been studied numerically. Dhole *et al.* [17] investigated the flow of a shear-thickening fluid past a falling sphere at intermediate to high Reynolds numbers ($10 < Re < 500$). By using a power-law model, they showed that the drag coefficient of shear-thickening systems is higher than the Newtonian counterparts at a given Reynolds number. The power-law viscosity can be expressed as $\eta = K \dot{\gamma}^{n-1}$, where K and n are the consistency factor and the power-law index with $n > 1$ for shear-thickening fluids. Despite these limited experimental and numerical efforts, it is still unclear how shear-thickening behavior could modify the exact form of flow structure around a falling sphere. In addition, the relevant theoretical results, in particular the reported drag enhancement by Dhole *et al.* [17], has not been verified in experiments.

Shear-thickening behavior has been documented in a wide range of micellar solutions at low concentrations [21–23]. Different characteristic methods such as small angle neutron scattering [24], birefringence [21], transmission electron microscopy imaging [25], and particle image velocimetry [26,27] combined with rheometry have been used to investigate different aspects of flow of shear-thickening micellar solutions. The shear-thickening phenomenon in surfactant solutions has been related to formation of shear-induced structures [28,29]. The dilute micellar solutions typically contain isolated rodlike micelles at equilibrium; however, beyond a critical imposed shear rate (which depends on micelles concentrations and temperature), the micelles can grow to form larger aggregates that in turn gives rise to viscoelastic effects [30,31].

Thus far, studies on flow of surfactant solutions past a falling sphere have mainly focused on a semidilute concentration regime in which long and flexible wormlike micelles exist [11–14,32–35]. Wormlike micelles are usually made by dissolving surfactants and salts in water. At high salt and surfactant concentrations, spherical micelles transform to long flexible wormlike structures that, at sufficiently high concentrations, entangle and induce shear-thinning viscoelastic responses [36]. Similar to shear-thinning viscoelastic polymer solutions, a negative wake has been reported in the rear of the falling sphere in wormlike micelles [11,13,33]. One interesting difference between sphere sedimentation results in wormlike micelles and polymeric solutions is that falling spheres may experience an instability in wormlike micelles that is characterized by acceleration and deceleration in sphere sedimentation velocity [11–14,32]. Such instabilities have been attributed to flow-induced micellar chain scission in the wake of the sphere where extensional flow is dominant [11,13]. Recently Mohammadigoushki and Muller proposed a phase diagram based on extensional Deborah number De_E and Reynolds number to distinguish steady from unsteady sphere sedimentation

behaviors [11]. De_E is defined as $De_E = \lambda \dot{\epsilon}_{\max}$, where λ is the Maxwell relaxation time and $\dot{\epsilon}_{\max}$ is the maximum strain rate in the wake of the falling sphere [11], and Re is defined as $Re = \rho \dot{\gamma} a^2 / \eta(\dot{\gamma})$.

Surfactant micellar solutions provide a unique platform for studies of shear-thickening fluids past a falling sphere, because unlike shear-thickening corn-starch suspensions, these systems are transparent and allow us to fully resolve the flow field around the falling sphere. The main goal of this study is to investigate the flow of a shear-thickening dilute micellar fluid past a falling sphere via a combination of particle tracking velocimetry and particle image velocimetry. In particular, the effect of shear thickening on sphere drag coefficient and form of flow structure around the falling sphere will be examined.

II. MATERIALS AND METHODS

In this work, the aqueous micellar solution contains hexadecyltrimethylammonium bromide (CTAB) and 5-methyl salicylic acid (5mS). The concentrations of CTAB and 5mS are 12.5 mM, and 7 mM, respectively. Both CTAB and 5mS were purchased from Sigma-Aldrich and used without further purification. The steady shear viscosity is measured via an Anton-Paar rheometer (model MCR 302) in a standard Couette coaxial cylinders geometry with inner cylinder of radius $R_i = 13.35$ mm and outer cylinder of radius $R_o = 14.53$ mm. Due to the importance of the extensional flows in the wake of the falling sphere, we have also performed transient extensional flow measurements via a custom-made capillary extensional rheometer (CaBER). More details about the CaBER device can be found in our recent work [37,38].

Sphere sedimentation experiments are performed in a cylindrical glass tube with length $L = 100$ cm and diameter $R = 85$ mm. A temperature-controlled water bath is used to keep the temperature of the micellar solution constant during sphere sedimentation experiments. Two types of spheres with different densities (nylon and Delrin[®]) and diameter ($a = 1/32$ – $1/4$ inches) are used in these experiments. These two types of spheres provide the least deviation from solution density, which in turn allow us to perform sphere sedimentation experiments over a broad range of Reynolds number. The micellar solution is seeded with 0.02 wt% seeding particles (model 110PB provided by Potters Industries LLC), and a laser (model Genesis MX 532-5000 from Coherent Inc.) is used to illuminate the flow field around the falling sphere. Sphere motion is recorded via a CCD camera (model STC-MBS241U3V) equipped with a AF-SDX Micro NIKKOR lens. The sphere velocity is obtained by tracking the sphere center of mass via an open source ImageJ Plugin [39]. Finally, to resolve the detail form of flow structure around the falling sphere, we performed particle image velocimetry analysis via an open source MATLAB code [40].

III. RESULTS

A. Steady shear rheology

To evaluate the viscoelastic response of the micellar solution, we performed small amplitude oscillatory shear (SAOS) experiments in the linear viscoelastic regime. The SAOS results showed very small storage modulus (below the lower limit of the rheometer) in a wide range of angular frequencies (results not shown). This indicates that in this solution micelles are not entangled, and therefore, solution behaves as a viscous fluid. This is consistent with the results of Davis *et al.* [23]. Moreover, in order to confirm the shear-thickening nature of the CTAB/5mS micellar solution, we have performed steady shear experiments. Figure 1 shows the steady-state shear viscosity (η) as a function of shear rate ($\dot{\gamma}$) for this micellar solution. At low shear rates, the shear viscosity is constant and about 0.02 Pa·s. However, for $\dot{\gamma} > 0.4$ (1/s), an upturn in viscosity is observed until viscosity reaches a maximum around 0.15 Pa·s for a shear rate of $\dot{\gamma} \approx 1.5$ (1/s). Therefore, this micellar solution shows an apparent shear-thickening behavior. The apparent shear-thickening behavior has been documented in a wide range of dilute micellar solutions and has been linked to flow-induced structure formation [21,22,41]. We will further discuss these results in Sec. IV.

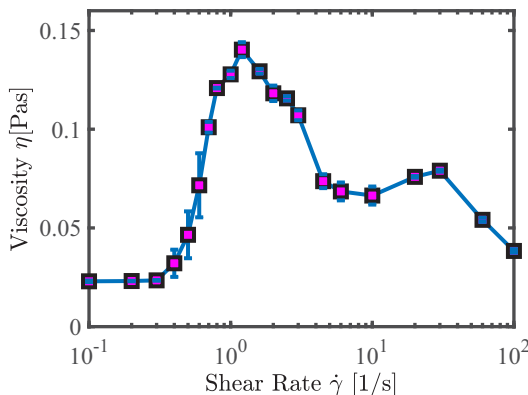


FIG. 1. Steady-state shear viscosity as a function of shear rate for a dilute micellar solution of CTAB/5mS at room temperature.

B. Transient extensional rheology

Sphere sedimentation dynamics is directly connected to the strong extensional flows in the rear of the sphere. Therefore, in addition to shear rheology, we have characterized extensional rheology of the micellar solution in a Capillary Breakup Extensional Rheometer (CaBER). Figure 2 shows a series of snapshots illustrating the filament-thinning dynamics in the micellar solution in CaBER experiments. Shortly after the strike time, a cylindrical fluid filament forms between the two plates and gradually thins. As time progresses, a beads-on-string phenomenon appears until eventually fluid filament pinches off. The beads-on-string phenomenon has been linked to inertio-capillary-thinning dynamics in a viscoelastic polymer solution [42,43]. To evaluate the importance of inertia in CaBER experiments, we can construct the ratio of the viscous timescale to the inertial timescale in CaBER experiments as

$$\frac{t_v}{t_i} = \frac{14.1\eta_0 R_0/\sigma}{1.95(\rho R_0^3/\sigma)^{1/2}}. \quad (1)$$

Using the experimental parameters of this study, $t_v \approx 0.63 t_i$. This indicates that inertia is important. Therefore, consistent with theory, the beads-on-string phenomenon is expected in the CaBER experiments with this dilute micellar solution.

Figure 3(a) shows temporal evolution of the normalized filament diameter for the micellar solution obtained from snapshots of Fig. 2. It turns out that the filament lifetime in CaBER experiments is on average about 26 ± 4 sec. The filament lifetime in CaBER experiments refers

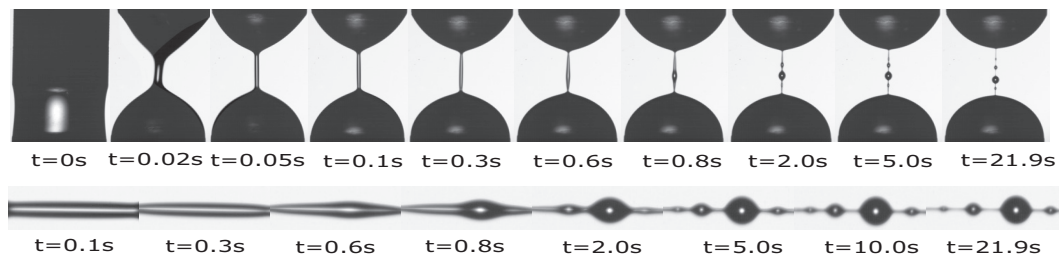


FIG. 2. Snapshots illustrating the filament-thinning process in the CaBER experiments for a CTAB/5mS solution. The lower panel shows a close-up view of the cylindrical filament that clearly indicates formation of the beads-on-string phenomenon.

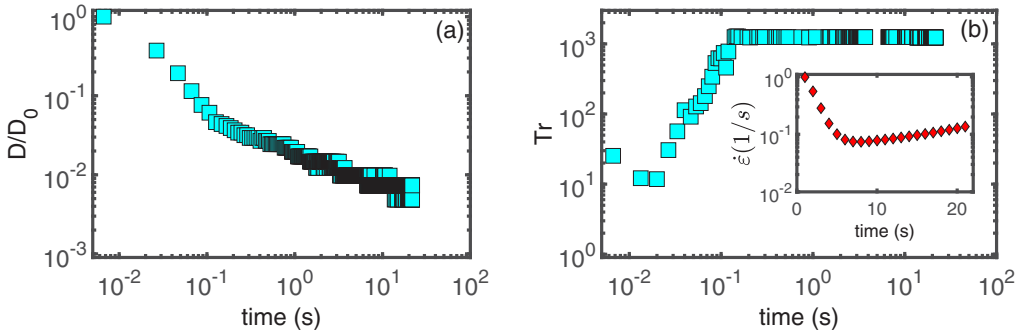


FIG. 3. (a) Normalized filament diameter as a function of time for a CTAB/5mS solution in CaBER experiments. (b) Transient Trouton ratio as a function of time. The inset in panel (b) shows the transient strain rate as a function of time.

to the window from cessation of uniaxial stretching till the filament pinch-off moment. In addition, Fig. 3(b) shows the Trouton ratio as a function of time for this micellar solution. It is clear that the Trouton ratio increases as a function of time until it reaches an asymptotic value around 1.3×10^3 . Finally, plotted in the inset of Fig. 3(b) is the strain rate profile during the filament-thinning process. The strain rate is calculated as $\dot{\epsilon} = \frac{-2}{D} \frac{dD}{dt}$. We will provide a detailed discussion of the above results in Sec. IV.

C. Particle tracking velocimetry

Following fluid characterization, we performed sphere sedimentation experiments and measured the temporal evolution of velocity of the sphere center of mass. Unlike previous experiments on wormlike micelles where a transition from steady to unsteady settling is reported, sphere sedimentation experiments in this dilute micellar solution show steady settling velocity over the entire range of experimental conditions. Perhaps this is not surprising, because this micellar system mainly consists of unentangled rodlike micelles that exhibit no viscoelasticity at equilibrium. Figure 4(a) shows representative velocity profiles as a function of time for series of spheres. We note that the surface chemistry of these spheres does not affect the sphere sedimentation dynamics in these experiments because (1) sphere sedimentation experiments are repeatable in both nylon and Delrin and (2) micellar solution rheology does not change after performing extensive sphere

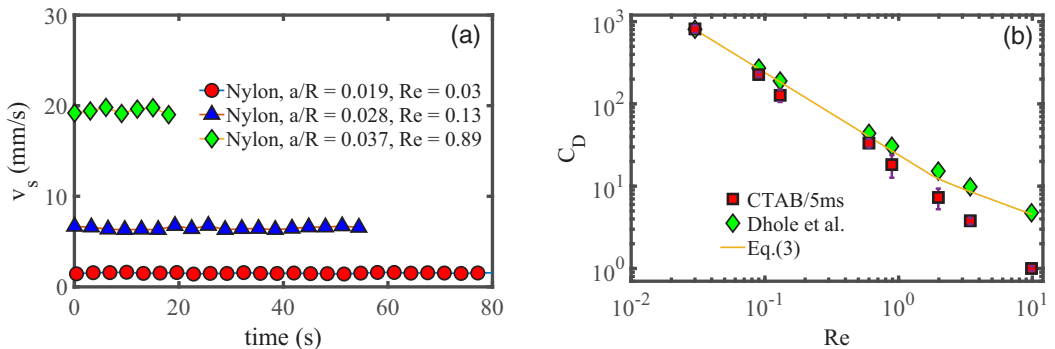


FIG. 4. (a) Velocity of the sphere center of mass as a function of time in a dilute micellar solution. (b) Drag coefficient as a function of Reynolds number for falling spheres in a CTAB/5mS solution (\square), in simulations of Dhole *et al.* [17] (\diamond), and in Newtonian fluids (continuous curve).

sedimentation experiments. The steady-state velocity data are used to calculate the total sphere drag coefficient. The total drag coefficient for the falling sphere in the micellar solution can be calculated from the force balance as [44]

$$C_D = \frac{4}{3} \frac{(\rho_s - \rho) ag}{\rho v_s^2}, \quad (2)$$

where ρ is the density of the solution, and ρ_s is the density of the sphere. Figure 4(b) shows the total drag coefficient as a function of Reynolds number for experiments in micellar solutions (squares) along with expected values for the Newtonian fluid (continuous curve) and simulations of Dhole *et al.* [17] (diamonds) for the power-law model with $n = 2$. We note that the total drag coefficient for a Newtonian fluid past a falling sphere is calculated as [44]

$$C_D \approx \begin{cases} 24/\text{Re}, & \text{if } \text{Re} < 1 \\ 18/\text{Re}^{0.6}, & \text{if } \text{Re} \geq 1 \end{cases}. \quad (3)$$

Simulation results of Dhole *et al.* [17] indicate that shear thickening leads to drag enhancement. The power-law index of $n = 2$ is similar to that the shear-thickening behavior in the micellar solution over the shear rate range of $0.5 \leq \dot{\gamma} \leq 1.5$ (1/s). Therefore, the sphere sedimentation experiments in a micellar solution are expected to generate a similar drag enhancement. However, at low inertia ($\text{Re} \approx 0.03$), the sphere drag in a micellar solution is similar to the one estimated by the Newtonian relation. More interestingly, as inertia increases to $\text{Re} \geq 0.09$, the drag coefficient in a micellar solution becomes smaller than the one for the Newtonian fluid. Therefore, despite the shear-thickening nature of this micellar solution, a drag reduction is reported at finite inertia. The latter result seems to be inconsistent with the simulation results of Dhole *et al.* [17] that shear thickening should lead to drag enhancements. Clearly, such drag reductions should be intimately connected to the structure of the flow around the falling sphere.

D. Particle image velocimetry

Particle image velocimetry (PIV) is performed to resolve the flow field around the falling sphere. Figure 5 shows the normalized velocity vectors around a falling sphere in a CTAB/5mS solution for nylon spheres with different sizes over a wide range of inertia Re . As expected, the velocity near the sphere surface is maximum and quickly reduces to zero upstream of the sphere center of mass. However, downstream of the sphere, velocity vectors decrease rather gradually.

Figures 6(a) and 6(b) show the normalized velocity of the fluid along the axis of the sphere center of mass parallel to the direction of the sphere motion. Fluid velocity is normalized by dividing to the velocity of the sphere center of mass. These results clearly show that the velocity profile around the sphere is no longer fore-aft-symmetric. Upstream of the sphere center of mass, velocity quickly drops to zero ($x \approx 15a$). Conversely, fluid velocity shows a rather gradual decay downstream of the sphere center of mass. For most cases, the velocity of the fluid does not approach zero even at distances about $80a$ away from the rear of the sphere. Included in Fig. 6 are the simulations of COMSOL multiphysics for the same size sphere and a shear-thickening power-law model with $n = 2$ (continuous curves). This shear-thickening index is chosen because it matches the one estimated from the shear-thickening portion of Fig. 1. The simulation results for the power-law model also show a modest wake which is further extended away from the sphere center of mass. Although this trend is consistent with the experimental results on the micellar solution, simulations significantly underestimate the experimental velocity profiles both upstream and downstream of the sphere center of mass. Therefore, we can conclude that the flow structure around the falling sphere in the dilute micellar solution is not solely described by the shear-thickening power-law effect. This conclusion is consistent with the above results on drag coefficient. The drag coefficient for spheres falling in a micellar solution is also significantly different from the one calculated for shear-thickening power-law fluids.

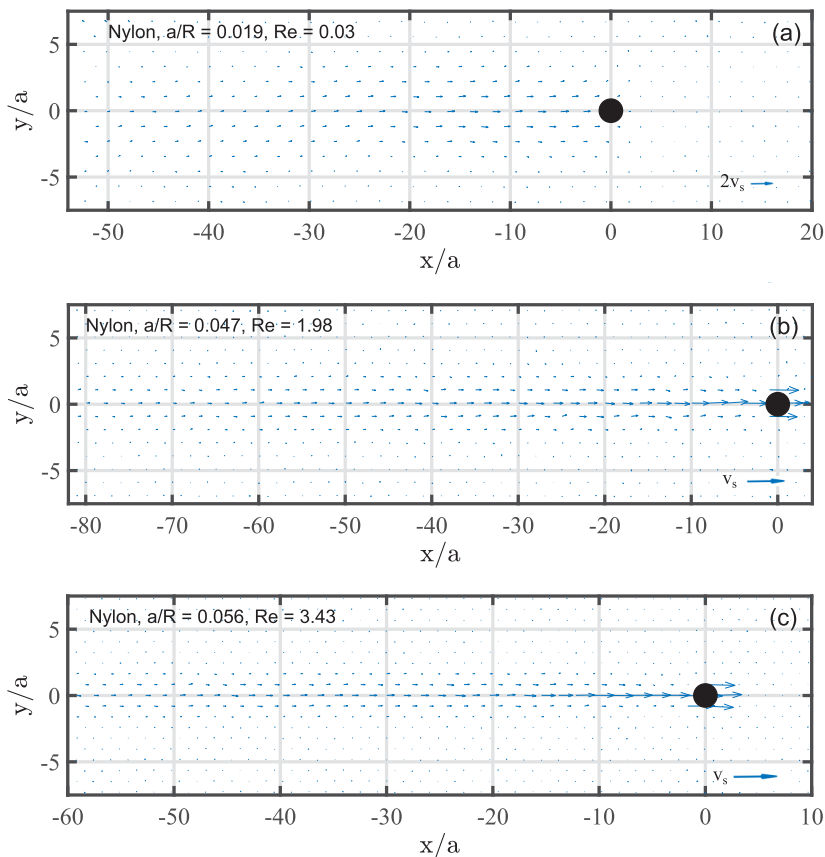


FIG. 5. Normalized velocity vector maps for nylon spheres falling in the dilute CTAB/5mS micellar solution at different Reynolds numbers.

To summarize, we illustrated that a sphere falling in the dilute CTAB/5mS micellar solution (12.5 mM/7 mM) experiences a drag reduction over a wide range of inertia Re . Additionally, the flow structure around the falling sphere is asymmetric with a strong extended wake in the rear of the sphere. In the following, we attempt to rationalize these seemingly unusual results.

IV. DISCUSSION

We start the discussion with particle tracking velocimetry results that indicated a strong drag reduction in the dilute micellar solution. A similar drag reduction has been documented in flow of viscoelastic polymer solutions and wormlike micelles past a falling sphere [9,11–13]. It is worth noting that there are two main differences between the experiments reported in this paper and prior pertaining experiments in viscoelastic fluids. First, the micellar solution studied in this work consists of unentangled rodlike micelles suspended in aqueous solution that do not exhibit any signs of viscoelasticity in a linear viscoelastic regime [23,25]. Second, viscoelastic systems show either a shear-thinning or constant-viscosity elastic behavior (Boger fluids), while the micellar solution in this study exhibits a strong shear thickening at low shear rates followed by shear thinning at high shear rates.

As noted in Fig. 1, the dilute CTAB/5mS micellar solution exhibits a strong shear-thickening behavior. At low shear rates [$\dot{\gamma} < 0.4$ (1/s)], the solution shows a constant viscosity, which

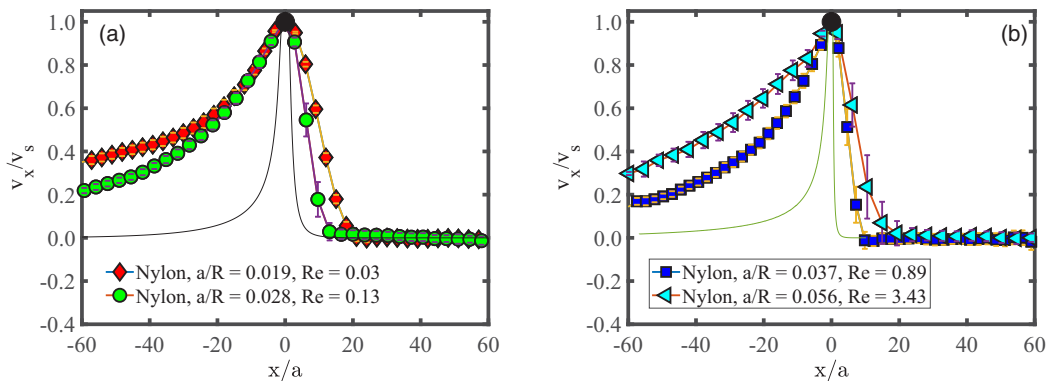


FIG. 6. Normalized steady-state velocity of the dilute CTAB/5mS micellar fluid on the sphere axis parallel to the direction of sphere motion. The continuous curves show the steady-state velocity of a shear-thickening power-law model with power-law index $n = 2$ as calculated by COMSOL.

indicates that micelles maintain their rodlike structure. However, as the imposed shear rate increases to $\dot{\gamma} \geq 0.4$ (1/s), rodlike micelles can fuse into each other and form larger aggregates of wormlike micelles. The presence of such wormlike micelles aggregates in solution can explain the increase in shear viscosity. At still higher shear rates [$\dot{\gamma} \geq 1.5$ (1/s)], the shear-induced structure exhibits a strong shear-thinning behavior. This shear-thinning behavior could be due to either alignment of the wormlike micelles in the direction of flow or flow-induced micellar breakage. Therefore, there clearly exists a positive feedback loop between flow and the micelles morphology, whereby flow can modify the microstructure of the micelles and micellar microstructure can in turn modify the flow field.

The significant drag reduction and presence of long extended wake in the rear of the falling spheres could be linked to flow-induced structure formation in this dilute micellar solution. Short rodlike micelles may have been affected by the strong flows around and in the wake of the falling sphere. The flow field around a falling sphere is complex in nature. On the flanks of the sphere and parallel to the direction of the sphere motion, a combination of shear deformation and extensional flow is present. However, in the wake of the falling sphere, extensional flow is dominant. Therefore, in the discussion to follow, we will assess the strength of the shear and extensional flows around the sphere by comparing the range of imposed shear rates and extension rates to that of applied to micellar solutions in simple shear and/or uniaxial extensional flows. Such comparisons will allow us to predict whether flow-induced structure formation could play any role in sphere sedimentation experiments.

To evaluate the strength of the shear flow around the falling sphere, the characteristic shear rates are calculated and listed in Table I. It is clear that such characteristic shear rates fall within the shear-thickening and shear-thinning portion of the steady shear viscosity data of Fig. 1. This indicates that the shear flow on the flanks of sphere is strong enough to transform rodlike micelles into long flexible wormlike micelles. The presence of wormlike micelles around the falling sphere should reduce the total drag. This provides what we believe is the first indirect evidence for formation of giant wormlike micellar aggregates in strong flows near the falling sphere.

In addition to shear deformation, the dynamics of the sphere sedimentation is linked to extensional flows that are dominant downstream of the sphere. The reported extended wake in the rear of sphere is reminiscent of the thin extended wake reported in flow of Boger fluids past a falling sphere [10]. Such extended wakes have been linked to elastic forces that can be carried over long distances by polymer chains. Although at equilibrium the micellar solution consists only of rodlike micelles with an average length shorter than 20 nm [23], a strong extensional flow can also perturb the micellar microstructure through elongation-induced structures (EISs) [37,45]. To evaluate

TABLE I. Spheres and corresponding flow parameters.

Material	a (inches)	Re	$\dot{\gamma}$ (1/s)	$\dot{\epsilon}_{\max}$ (1/s)
Nylon	1/16	0.03	1.07	0.02
Delrin	1/16	0.09	3.86	0.19
Nylon	3/32	0.13	2.60	0.08
Delrin	3/32	0.6	7.91	0.28
Nylon	1/8	0.89	5.99	0.39
Nylon	5/32	1.98	8.44	0.57
Nylon	3/16	3.43	10.45	0.81
Nylon	1/4	9.86	17.60	1.94

this hypothesis, we have characterized the extensional flow along the axis of the sphere center of mass.

Figures 7(a) and 7(b) show the strain rate along the axis of sphere center of mass, parallel to the direction of sphere motion. The strain rate is calculated as

$$\dot{\epsilon}_{xx} = dv_x/dx. \quad (4)$$

The general features of the strain rate profiles are the same for different experiments. Upstream of the sphere center of mass, the strain rate decreases and shows negative signs as we move closer to the sphere center of mass. This is mainly because in the leading edge of the sphere, flow is

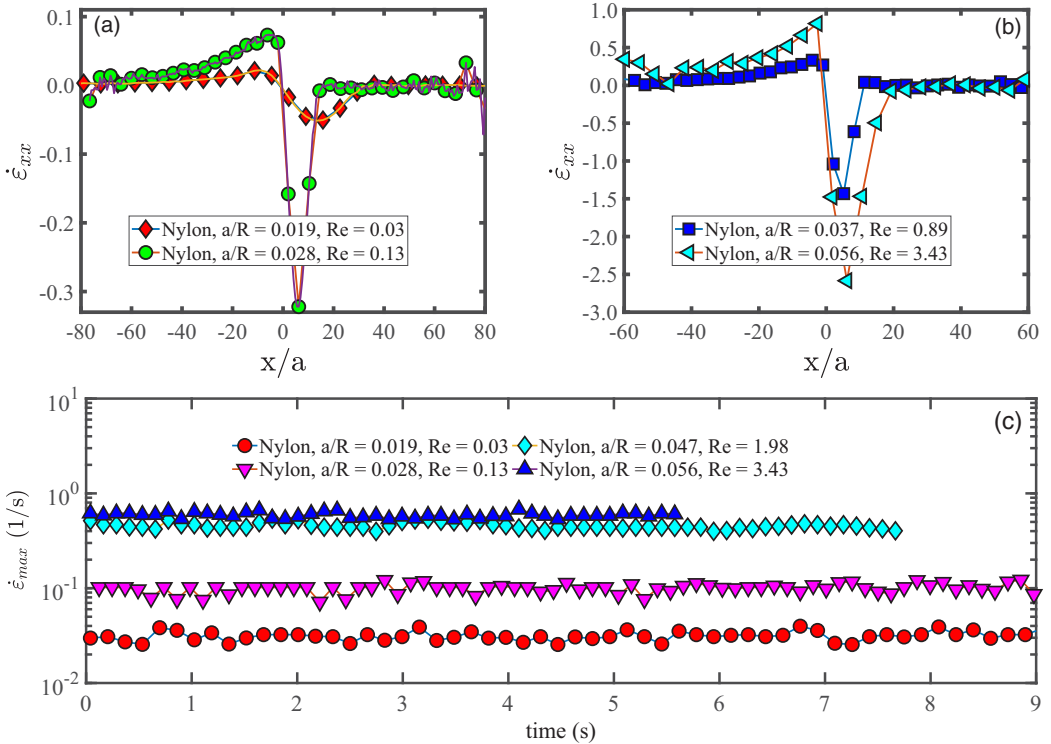


FIG. 7. (a), (b) Strain rate as a function of distance from the sphere center of mass. (c) Temporal evolution of maximum wake strain rate ($\dot{\epsilon}_{\max}$) for different spheres over a wide range of inertia.

mostly compressive. However, as we move further downstream of the sphere, the strain rate shows a maximum followed by a decay to zero. The maximum strain rate $\dot{\epsilon}_{\max}$ remains almost constant over the course of sphere sedimentation experiments for all experiments reported in this study. Figure 7(c) shows the maximum strain rate as a function of time in these experiments. As the particle inertia (Re) increases, the maximum strain rate in the wake of the sphere increases. The averaged maximum strain rate for each experiment is listed in Table I. In addition, a sample movie in the Supplemental Material [46] presents the velocity vectors, strain rate, and velocity along the center line of the falling sphere. To evaluate the strength of the extensional flows in the rear of the falling spheres, we compare the maximum strain rates in the rear of the sphere presented in Fig. 7(c) to the ones calculated from uniaxial extensional experiments of CaBER [inset of Fig. 3(b)]. Except for the smallest nylon sphere with $Re = 0.03$, the strain rates that are listed in Table I lie within the range of strain rates imposed by CaBER device. This means that the extensional flow in the wake of the sphere for most cases is as strong as the extensional flow imposed by CaBER. Therefore, if EISs can occur in experiments with CaBER, we expect a similar phenomenon to occur in sphere sedimentation experiments.

To examine EIS formation in CaBER experiments, we return to the results of Fig. 3. For a Newtonian fluid, the midfilament diameter decays linearly with time filament as

$$D(t) = D_0 - 0.1418 \frac{\sigma}{\eta_s} t, \quad (5)$$

where D_0 , η_s , and σ are the diameter of the plates, viscosity of the solvent (here water), and surface tension. Using this equation, we can calculate a filament lifetime of about 12 ms for a Newtonian fluid with a viscosity equivalent to the zero-shear viscosity of the surfactant micellar solution. Therefore, the filament lifetime of the dilute micellar solution is much larger than the filament lifetime of a Newtonian fluid at a given zero-shear viscosity. More importantly, the maximum Trouton ratio (Tr_{∞}) in the CaBER experiment with this micellar solution is much higher than the Newtonian counterpart ($Tr = 3$). In fact, similar results have been reported in the past for other shear-thickening micellar solutions in the range of the dilute concentration regime [37,45]. In the CaBER experiments micellar fluid is subject to a strong perturbation at the onset of experiments when the step strain is imposed. Such strong initial perturbations could potentially modify the equilibrium micellar microstructure. To connect the dynamic micellar microstructure to the parameters measured in extensional flows, we invoke a similar finitely extensible nonlinear elastic (FENE-P) analysis used by Omidvar *et al.* [37]. According to the asymptotic analysis of the FENE-P model, the steady-state extensional viscosity can be written as [47]

$$\eta_{E,\infty} - 3\eta_s = 2nk_B T \lambda L^2 [1 - 1/(2\lambda\dot{\epsilon}) + \dots], \quad (6)$$

where $\eta_{E,\infty}$, η_s , n , K_B , T , λ , and L^2 are maximum extensional viscosity, solvent viscosity, surfactant concentration per unit volume, Boltzmann constant, temperature, relaxation time, and dimensionless finite extensibility parameter. The dimensionless finite extensibility parameter is defined as $L^2 = Q^2/\langle Q_{eq}^2 \rangle$, where Q is the maximum attainable micellar length in extensional flows and $\langle Q_{eq} \rangle$ is the equilibrium micellar length. For CaBER experiments, the nominal extension rate is considered as $\dot{\epsilon} = 2/3\lambda$. In addition, $\eta_{E,\infty} \gg \eta_s$ for this micellar solution. Therefore, Eq. (6) can be simplified further as

$$\eta_{E,\infty} \approx G\lambda L^2/2, \quad (7)$$

where elastic modulus G is given by $G = nK_B T$ and can be estimated as $\lambda = \eta_0/G$. This gives a relation between Trouton ratio and the finite extensibility parameter as $L^2 = 2Tr_{\infty}$. The latter relation connects the micellar microstructure to the extensional rheological parameters. Substituting for the numerical value of Tr_{∞} , we can calculate the finite extensibility parameter of the micelles as $L^2 = 2.6 \times 10^3$. On the other hand, according to the experimental neutron scattering data of Davies *et al.* [23], the CTAB/5mS micellar solution (12.5 mM/10 mM) at room temperature forms short, rodlike micelles with an average length about 20 nm. The CTAB/5mS micellar solution

(12.5 mM/7 mM) should contain smaller micelles than the CTAB/5mS (12.5 mM/10 mM) due to its lower zero-shear viscosity. Using 20 nm as an upper limit for equilibrium micellar length in combination with the estimated finite extensibility parameter, we can estimate the final length of the micelles in the CaBER experiment as $\approx 1 \mu\text{m}$. We note that micelles themselves do not have the necessary length to undergo such big extensions. The only possible way to generate such big finite extensibility is through aggregation of cylindrical micelles into big wormlike micelles under extensional flows, i.e., EISs. Therefore, based on this analysis, strong extensional flows in CaBER have induced a transition from short rodlike micelles to long flexible wormlike structures. Thus, in sphere sedimentation experiments, where extensional flows are as strong as CaBER experiments, micelles should also experience a similar EIS. This provides further support that the sphere drag reduction and the extended wake downstream of the falling sphere in the dilute micellar solution are linked to EIS formation. In addition to CaBER experiments, we attempted to evaluate the orientation and microstructure of the micelles around the falling spheres using birefringent experiments. Our results indicate that the micellar solution around the falling sphere does not show measurable birefringence, presumably due to the weak nature of birefringent patterns. Although the CaBER analysis provides an indirect evidence for EIS formation in sphere sedimentation experiments in a dilute micellar solution, further microstructural analysis with scattering techniques (e.g., small angle neutron or small angle x-ray) is necessary to obtain direct evidence for EIS formation.

V. CONCLUSIONS

To conclude, we studied dynamics of a falling sphere in a shear-thickening dilute micellar solution based on CTAB/5mS (12.5 mM/7 mM) at room temperature. Particle tracking velocimetry illustrated a significant drag reduction in this micellar solution over a wide range of inertia $0.09 \leq \text{Re} \leq 9.86$. In addition, detailed PIV analysis showed that a long extended wake forms in the rear of the falling sphere. These results suggest that the strong flow around the falling sphere has modified the micellar microstructure by inducing a transition from rodlike to flexible wormlike structures. The presence of wormlike micelles will significantly modify the sphere sedimentation dynamics. This hypothesis is in line with transient capillary breakup extensional measurements that demonstrated signatures of EIS formation in this micellar solution.

-
- [1] R. G. Owens and T. N. Phillips, *Computational Rheology*, Vol. 14 (World Scientific, Singapore, 2002).
 - [2] R. Zenit and J. J. Feng, Hydrodynamic interactions among bubbles, drops, and particles in non-Newtonian liquids, *Annu. Rev. Fluid Mech.* **50**, 505 (2018).
 - [3] R. P. Chhabra, *Bubbles, Drops, and Particles in Non-Newtonian Fluids* (CRC Press, Boca Raton, FL, 2006).
 - [4] M. M. Mrokowska and A. Krzto-Maziopa, Viscoelastic and shear-thinning effects of aqueous exopolymer solution on disk and sphere settling, *Sci. Rep.* **9**, 7897 (2019).
 - [5] M. T. Arigo and G. H. McKinley, An experimental investigation of negative wakes behind spheres settling in a shear-thinning viscoelastic fluid, *Rheol. Acta* **37**, 307 (1998).
 - [6] M. Bush, On the stagnation flow behind a sphere in a shear-thinning viscoelastic liquid, *J. Non-Newtonian Fluid Mech.* **55**, 229 (1994).
 - [7] J. Mendoza-Fuentes, A. R. Montiel, R. Zenit, and O. Manero, On the flow of associative polymers past a sphere: Evaluation of negative wake criteria, *Phys. Fluids* **21**, 033104 (2009).
 - [8] O. G. Harlen, The negative wake behind a sphere sedimenting through a viscoelastic fluid, *J. Non-Newtonian Fluid Mech.* **108**, 411 (2002).
 - [9] M. T. Arigo and G. H. McKinley, The effects of viscoelasticity on the transient motion of a sphere in a shear-thinning fluid, *J. Rheol.* **41**, 103 (1997).

- [10] D. Fabris, S. J. Muller, and D. Liepmann, Wake measurements for flow around a sphere in a viscoelastic fluid, *Phys. Fluids* **11**, 3599 (1999).
- [11] H. Mohammadigoushki and S. J. Muller, Sedimentation of a sphere in wormlike micellar fluids, *J. Rheol.* **60**, 587 (2016).
- [12] S. Wu and H. Mohammadigoushki, Sphere sedimentation in wormlike micelles: Effect of micellar relaxation spectrum and gradients in micellar extensions, *J. Rheol.* **62**, 1061 (2018).
- [13] S. Chen and J. P. Rothstein, Flow of a wormlike micelle solution past a falling sphere, *J. Non-Newtonian Fluid Mech.* **116**, 205 (2004).
- [14] A. Jayaraman and A. Belmonte, Oscillations of a solid sphere falling through a wormlike micellar fluid, *Phys. Rev. E* **67**, 065301(R) (2003).
- [15] M. Arigo, D. Rajagopalan, N. Shapley, and G. H. McKinley, The sedimentation of a sphere through an elastic fluid. Part 1. Steady motion, *J. Non-Newtonian Fluid Mech.* **60**, 225 (1995).
- [16] D. Rajagopalan, M. Arigo, and G. H. McKinley, The sedimentation of a sphere through an elastic fluid. Part 2. Transient motion, *J. Non-Newtonian Fluid Mech.* **65**, 17 (1996).
- [17] S. D. Dhole, R. P. Chhabra, and V. Eswaran, Flow of power-law fluids past a sphere at intermediate Reynolds numbers, *Ind. Eng. Chem. Res.* **45**, 4773 (2006).
- [18] C. Rajasekhar Reddy and N. Kishore, Wall retardation effects on flow and drag phenomena of confined spherical particles in shear-thickening fluids, *Ind. Eng. Chem. Res.* **51**, 16755 (2012).
- [19] S. von Kann, J. H. Snoeijer, D. Lohse, and D. van der Meer, Nonmonotonic settling of a sphere in a cornstarch suspension, *Phys. Rev. E* **84**, 060401(R) (2011).
- [20] E. Verneuil, R. J. Phillips, and L. Talini, Axisymmetric two-sphere sedimentation in a shear thinning viscoelastic fluid: Particle interactions and induced fluid velocity fields, *J. Rheol.* **51**, 1343 (2007).
- [21] Y. Hu, S. Wang, and A. Jamieson, Rheological and flow birefringence studies of a shear-thickening complex fluid—A surfactant model system, *J. Rheol.* **37**, 531 (1993).
- [22] Y. Hu, P. Boltenhagen, and D. Pine, Shear thickening in low-concentration solutions of wormlike micelles. I. Direct visualization of transient behavior and phase transitions, *J. Rheol.* **42**, 1185 (1998).
- [23] T. S. Davies, A. M. Ketner, and S. R. Raghavan, Self-assembly of surfactant vesicles that transform into viscoelastic wormlike micelles upon heating, *J. Am. Chem. Soc.* **128**, 6669 (2006).
- [24] M. Takeda, T. Kusano, T. Matsunaga, H. Endo, M. Shibayama, and T. Shikata, Rheo-SANS studies on shear-thickening/thinning in aqueous rodlike micellar solutions, *Langmuir* **27**, 1731 (2011).
- [25] Z. Lin, J. Cai, L. Scriven, and H. Davis, Spherical-to-wormlike micelle transition in CTAB solutions, *J. Phys. Chem.* **98**, 5984 (1994).
- [26] B. M. Marín-Santibáñez, J. Pérez-González, L. De Vargas, F. Rodríguez-González, and G. Huelsz, Rheometry-PIV of shear-thickening wormlike micelles, *Langmuir* **22**, 4015 (2006).
- [27] E. R. Macias, F. Bautista, J. F. A. Soltero, J. E. Puig, P. Attane, and O. Manero, On the shear thickening flow of dilute CTAT worm-like micellar solutions, *J. Rheol.* **47**, 643 (2003).
- [28] R. Oda, P. Panizza, M. Schmutz, and F. Lequeux, Direct evidence of the shear-induced structure of wormlike micelles: Gemini surfactant 12-2-12, *Langmuir* **13**, 6407 (1997).
- [29] S. L. Keller, P. Boltenhagen, D. J. Pine, and J. A. Zasadzinski, Direct Observation of Shear-Induced Structures in Wormlike Micellar Solutions by Freeze-Fracture Electron Microscopy, *Phys. Rev. Lett.* **80**, 2725 (1998).
- [30] I. Wunderlich, H. Hoffmann, and H. Rehage, Flow birefringence and rheological measurements on shear induced micellar structures, *Rheol. Acta* **26**, 532 (1987).
- [31] J. F. Berret, R. Gamez-Corrales, Y. Serero, F. Molino, and P. Lindner, Shear-induced micellar growth in dilute surfactant solutions, *Europhys. Lett.* **54**, 605 (2001).
- [32] Y. Zhang and S. J. Muller, Unsteady sedimentation of a sphere in wormlike micellar fluids, *Phys. Rev. Fluids* **3**, 043301 (2018).
- [33] H. Mohammadigoushki and S. J. Muller, Creeping flow of a wormlike micelle solution past a falling sphere: Role of boundary conditions, *J. Non-Newtonian Fluid Mech.* **257**, 44 (2018).
- [34] M. Kostrzewa, A. Delgado, and A. Wierschem, Particle settling in micellar solutions of varying concentration and salt content, *Acta Mech.* **227**, 677 (2016).

- [35] Z. Wu and R. Zhanga, Learning physics by data for the motion of a sphere falling in a non-Newtonian fluid, *Commun. Nonlinear Sci. Numer. Sim.* **67**, 577 (2019).
- [36] C. A. Dreiss, Wormlike micelles: Where do we stand? Recent developments, linear rheology and scattering techniques, *Soft Matter* **3**, 956 (2007).
- [37] R. Omidvar, A. Dalili, A. Mir, and H. Mohammadigoushki, Exploring sensitivity of the extensional flow to wormlike micellar structure, *J. Non-Newtonian Fluid Mech.* **252**, 48 (2018).
- [38] R. Omidvar, S. Wu, and H. Mohammadigoushki, Detecting wormlike micellar microstructure using extensional rheology, *J. Rheol.* **63**, 33 (2019).
- [39] H. Ewers, A. E. Smith, I. F. Sbalzarini, H. Lilie, P. Koumoutsakos, and A. Helenius, Single-particle tracking of murine polyoma virus-like particles on live cells and artificial membranes, *Proc. Natl. Acad. Sci. USA* **102**, 15110 (2005).
- [40] W. Thielicke and E. J. Stamhuis, Pivlab-towards user-friendly, affordable and accurate digital particle image velocimetry in MATLAB, *J. Open Res. Softw.* **2**, e30 (2014).
- [41] C.-h. Liu and D. J. Pine, Shear-Induced Gelation and Fracture in Micellar Solutions, *Phys. Rev. Lett.* **77**, 2121 (1996).
- [42] L. E. Rodd, T. P. Scott, J. J. Cooper-White, and G. H. McKinley, Capillary break-up rheometry of low-viscosity elastic fluids, *Appl. Rheol.* **15**, 12 (2005).
- [43] C. Clasen, J. Eggers, M. A. Fontelos, J. Li, and G. H. McKinley, The beads-on-string structure of viscoelastic threads, *J. Fluid Mech.* **556**, 283 (2005).
- [44] M. M. Denn, *Process Fluid Mechanics* (Prentice Hall, New York, 1980).
- [45] D. Sachsenheimer, C. Oelschlaeger, S. Müller, J. Küstner, S. Bindgen, and N. Willenbacher, Elongational deformation of wormlike micellar solutions, *J. Rheol.* **58**, 2017 (2014).
- [46] See Supplemental Material at <http://link.aps.org/supplemental/10.1103/PhysRevFluids.4.073303> for a movie that shows the velocity vectors around a falling sphere in the shear thickening fluid and the resulting maximum strain rate in its wake.
- [47] P. S. Doyle, E. S. Shaqfeh, G. H. McKinley, and S. H. Spiegelberg, Relaxation of dilute polymer solutions following extensional flow, *J. Non-Newtonian Fluid Mech.* **76**, 79 (1998).